Acta Polytechnica CTU Proceedings **50**:18–23, 2024
https://doi.org/10.14311/APP.2024.50.0018

Published by the Czech Technical University in Prague

FINITE ELEMENT ANALYSIS OF NANOINDENTATION PILE-UP AND CORRECTION OF PROJECTED CONTACT AREA

Jaroslav Kovář[a,*], Vladimír Fuis[a,b], Radim Čtvrtlík[c], Jan Tomáštík[c]

[a] *Brno University of Technology, Institute of Solid Mechanics, Mechatronics and Biomechanics, Technická 2896/2 616 69 Brno, Czech Republic*

[b] *Czech Academy of Sciences, Institute of Thermomechanics, Centre of Mechatronics, Technická 2896/2; 619 69 Brno, Czech Republic*

[c] *Academy of Sciences of the Czech Republic, Institute of Physics, Joint Laboratory of Optics of Palacký University and Institute of Physics AS CR, 17. listopadu 50a, 772 07 Olomouc, Czech Republic*

[*] corresponding author: jaroslav.kovar@vut.cz

Abstract. This paper deals with the pile-up phenomenon that can occur during nanoindentation. Finite Element (FE) simulation of X5CrNiCuNb16-4 steel nanoindentation with pyramidal Berkovich indenter was done, and stress and strain beneath the indenter leading to pile-up behavior were analyzed in detail. Pile-up also influences the projected contact area, which should be corrected to include the pile-up into the Oliver-Pharr analysis. Accurate calculation of the projected contact area requires knowledge of its boundary. Few methods of boundary approximation were used, including approximation by the triangle and the semi-ellipse. For more precise approximation, the expression for parabolical approximation was derived. These methods were compared with the projected contact area calculated by finite element method. The most precise results were obtained using semi-elliptical and parabolical correction, which can be used for the determination of the projected contact area and its boundary.

Keywords: Nanoindentation, Berkovich indenter, pile-up, parabolical correction, steel, finite element method.

1. Introduction

Pile-up behavior can occur during the nanoindentation of soft, plastic materials. This leads to accumulation of plastically deformed material beneath the indenter and an increase in the contact area. The pile-up is maximal around the sides of the indenter and minimal under the indenter edges, see Figure 1.

Pile-up can significantly affect the results of Oliver-Pharr analysis (described in [1, 2]), but it is difficult to correct its influence on the projected contact area. This paper is aimed on modelling of X5CrNiCoNb16-4 nanoindentation by finite element method (FEM) and the description of the pile-up formation process from the mechanical perspective. Additionally, the commonly used corrections of the pile-up are unified and compared with FEM results and results calculated by new parabolical correction to get more accurate algorithm for describing pile-up.

2. Methods

2.1. FE model

To describe the pile-up, FE calculation was done for the nanoindentation of X5CrNiCoNb16-4 steel. The FE model similar to one, which was already described in [3], was employed. A blunted pyramidal Berkovich indenter with the tip radius of 400 nm was used for calculations. The indentation depth was 500 nm, which was 100 times smaller than the dimensions of specimen and indenter. According to [4], these dimensions should be enough to eliminate the influence of the specimen and indenter boundaries. Due to symmetry, only one-sixth of the geometry was modeled (Figure 2. The displacement along the z-axis at the bottom of the specimen and displacements perpendicular to the symmetry plane were fixed at them. The specimen was loaded by the displacement of the Berkovich indenter. In the first loadstep, a displacement 500 nm was applied on its top, followed by unloading in the second loadstep.

The diamond indenter was described by isotropic linear elastic model of material with Young's modulus $E_{dia} = 1\,141$ GPa and Poisson's ratio $\nu_{dia} = 0.07$. The steel was modeled using a multilinear model of material with $E_{steel} = 202$ GPa, $\nu_{steel} = 0.3$ and the yield strength $R_{esteel} = 500$ MPa. The stress-strain curve for this model has been defined by linearly interpolated 18 points (described in [3]) and the isotropic hardening was used.

The mesh was created from 3D SOLID 186 elements with the use of the contact CONTA 174 and TARGE 170 elements at contact area. To describe the pile-up around the contact area, the mesh was refined here. Totally was used 74 439 elements and the finest elements had approximately 2 nm. The contact was solved using the Augmented Lagrange algorithm with a coefficient of friction 0.1, whose impact has already been determined in [5]. After performing the calculations, the simulated indentation curve has been

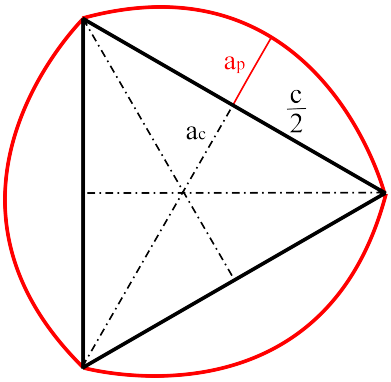

(A). Projection of the contact area at Berkovich indentation of the material with pile-up.

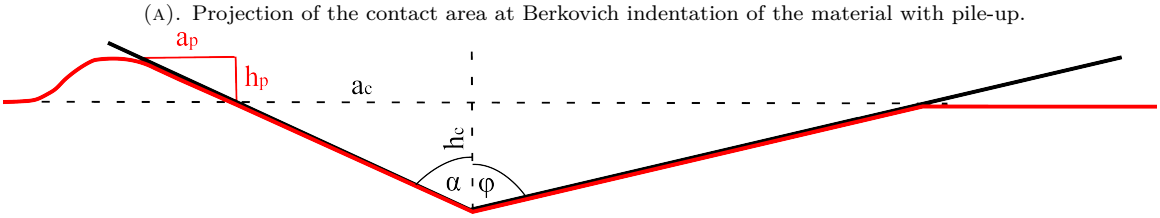

(B). Cross section of the soft material indent with Berkovich indenter.

FIGURE 1. Visualization of the pile up effect.

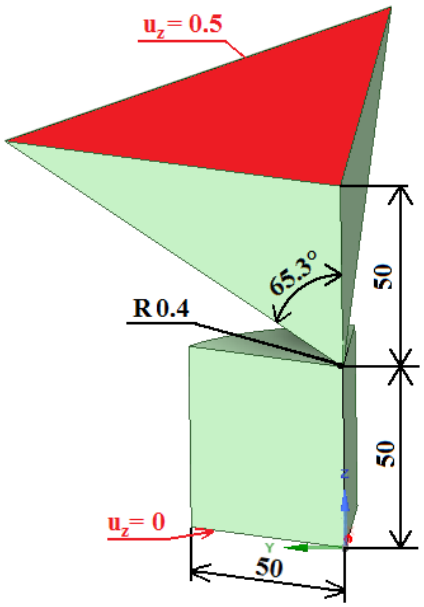

FIGURE 2. Model of geometry of Berkovich indentation used for FEM calculations [µm] with boundary conditions (at the section planes, the symmetry conditions were used).

compared with experimental data (described in [3] in detail).

2.2. Corrections of the pile-up

To calculate the precise results of Young's modulus and hardness by Oliver-Pharr analysis, the projected contact area has to be known. Few methods of its calculations will be compared in this paper.

2.2.1. Oliver-Pharr analysis

The commonly used Oliver-Pharr analysis was derived from the Sneddon solution, described in [6] which assumed only elastic deformations. As the pile-up is mainly caused by the plasticity, its influence is not included into the Oliver-Pharr analysis, which is only applicable to sink-in behavior, when the specimen surface bends under the indenter. The projected contact area in Oliver-Pharr analysis can be determined for the ideal Berkovich indenter according to Eq. (1). If the indenter is blunted, the projected contact area can be determined as the area of its cross-section at the contact depth h_c. To correct the results of Oliver-Pharr analysis for pile-up, the Eq. (2) is commonly used, where A_{OP} is area obtained by Oliver-Pharr analysis and A_p represents the correction for pile-up.

$$A_{OPideal} = 24.56 \cdot h_c^2 \tag{1}$$

$$A_c = A_{OP} + A_P \tag{2}$$

2.2.2. Triangular correction

The idea of approximation of pile-up region by triangle (Figure 3) was proposed by [7] and can be described by Eq. (3). For a Berkovich indenter, the c can be determined by Eq. (4) and with the use of Eq. (5) and the assumption of identical pile-ups on each indenter side, the pile-up area bounded by the triangle (A_{pt}) can be expressed by Eq. (6).

$$A_{pt} = \frac{1}{2 \cdot \tan(\frac{\pi}{2} - \alpha)} \cdot \sum_{i=1}^{3} h_{pi} \cdot c_i \tag{3}$$

$$c = 2 \cdot \sqrt{3} \cdot a_c \tag{4}$$

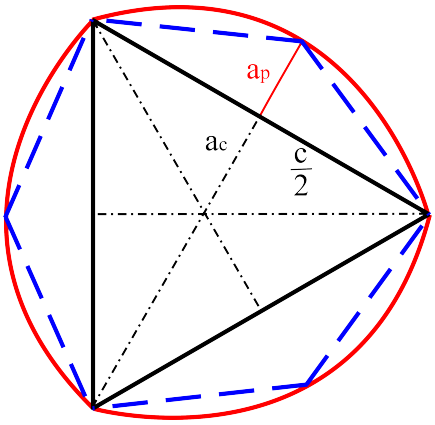

Figure 3. Approximation of the pile-up by triangles (red line represents the boundary of the pile-up area; blue line represents the boundary of the correction).

$$a_c = h_c \cdot \tan\alpha \tag{5}$$

$$A_{pt} = \frac{3 \cdot \sqrt{3} \cdot \tan\alpha}{\tan(\frac{\pi}{2} - \alpha)} \cdot h_c \cdot h_p \cong 24.562 \cdot h_c \cdot h_p \tag{6}$$

2.2.3. Semi-elliptical correction

To better describe the boundary of the pile-up, its approximation by semi-ellipse was derived by [8]. With this correction, the approximation of all pile-ups can be expressed by Eq. (7). If the indenter deformation is negligible, the Eq. (8) can be used, and the pile-up area can be given by Eq. (9). Although the semi-elliptical correction provides an accurate description, it can overestimate the pile-up near the indenter's edge due to the semi-elliptical shape (Figure 4).

$$A_{ps} = \frac{\pi \cdot c}{4} \cdot \sum_{i=1}^{3} a_{pi} \tag{7}$$

$$a_p = h_p \cdot \tan\alpha \tag{8}$$

$$\begin{aligned} A_{ps} &= \frac{3 \cdot \sqrt{3} \cdot \pi \cdot \tan^2\alpha}{2} \cdot h_c \cdot h_p \\ &\cong 38.582 \cdot h_c \cdot h_p \end{aligned} \tag{9}$$

2.2.4. Parabolical correction

Parabolical correction was derived to reduce the discrepancy near the indenter edges. This correction, which is described by [9], uses the approximation of the pile-up boundary by a parabola. For simplification, the equations for this correction were derived in the local coordinate system (Figure 5). The parabola passes through three points, two on the edges of the indenter (points A and C) and one which is the point of maximum pile-up in its center (point B). The coordinates of these points can be written by Eq. (10). By substituting these points into the general equation

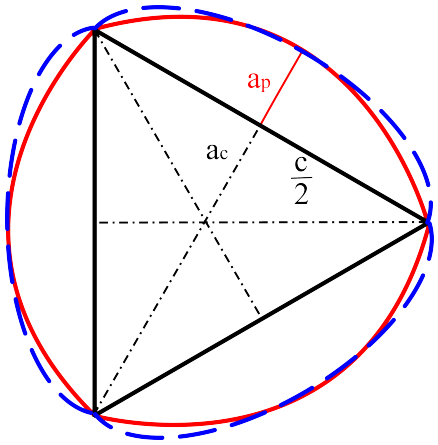

Figure 4. Approximation of the pile-up by semi-ellipses (red line represents the boundary of the pile-up area; blue line represents the boundary of the correction).

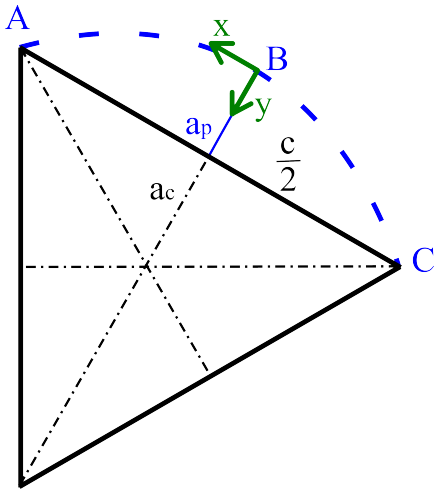

Figure 5. Approximation of the pile-up by parabola.

of parabola described by Eq. (11), the equation of the parabolical boundary described by Eq. (12) was derived.

The projection of the pile-up onto the plane of the specimen surface is bounded by the parabola on one side and the edge of the indent at the other side (Figure 5). This boundary can be expressed by Eq. (13). Assuming of its symmetry, the area of one pile-up can be described by Eq. (14). With the substitution of c and a_p from previous equations and assumption of the same pile-ups at all three sides of the indent, the total pile-up area can be described by Eq. (15).

$$A\left[\frac{c}{2}; a_p\right] \quad B\left[0; 0\right] \quad C\left[-\frac{c}{2}; a_p\right] \tag{10}$$

$$y = a_0 \cdot x^2 + b_0 \cdot x + c_0 \tag{11}$$

$$y_{b1} = a_p \cdot x^2 \cdot \left(\frac{c}{2}\right)^{-2} \tag{12}$$

$$y_{b2} = a_p \tag{13}$$

$$A_{pp1/3} = 2 \cdot \int_0^{\frac{c}{2}} \int_{y_{b1}}^{y_{b2}} 1 \; dy \; dx = \frac{4}{3} \cdot a_p \cdot \frac{c}{2} \tag{14}$$

$$A_{pp} = 4 \cdot \frac{\tan^2 \alpha}{\tan 30^\circ} \cdot h_c \cdot h_p \cong 32.748 \cdot h_c \cdot h_p \tag{15}$$

2.2.5. Finite element method

When the FEM is used, the elements in the contact may be selected and the projected contact area calculated as its surface after the projection onto the plane of the specimen surface. This area does not use any approximation of its boundary and if the mesh is enough fine, it can be used for the comparison of the other corrections. The procedure used in this paper is described in Chapter 4 in detail.

3. Pile-up

The FEM results confirmed that pile-up occurs during the steel nanoindentation. The location of the equivalent stress maximum was beneath the specimen surface, which was caused by the bluntness of the indenter. As the indentation depth grew, the plastic zone began to form (Figure 6). The results of plastic strain in the way of indentation showed a significant zone of compressive strain under the indenter but next this zone, the positive (tensile) values appeared, forming the pile-up region that grows with the indentation depth.

The tensile plastic strain is caused by the deformation of the specimen. At the beginning of the indentation, the material is compressed under the indenter, until the creation of plastic zone. Plastically deformed material has very limited ability of volumetric compressibility and begins to push surrounding material away, which leads to the creation of pile-up. This can be confirmed by the deformation of the specimen (Figure 7), where is shown how is the material in pile-up region pushed to the specimen under the indenter, but behind the side of indenter, the vector of deformation reverses, which describes the pushing the material away and forming pile-up.

When the indentation curves were determined by FEM, the Oliver-Pharr analysis was used to calculate the contact depth and its value $h_c = 472\,\text{nm}$ was obtained. As the Oliver-Pharr analysis does not include pile-up, it was expected that h_c should be 500 nm, what was the depth of indentation. This discrepancy was clarified by the plotting the detail of pile-up at indent profile (Figure 8). The profile can be divided into the three parts. The first one from the right is the steep line caused by the indenter profile (the graph is scaled to make details better visible). Then there is a pile-up region and at the bigger distance from the indent sink-in occurs too. This indicates that the influence of significant plasticity beneath the indenter tip becomes negligible further away from the indent, making sink-in the dominant

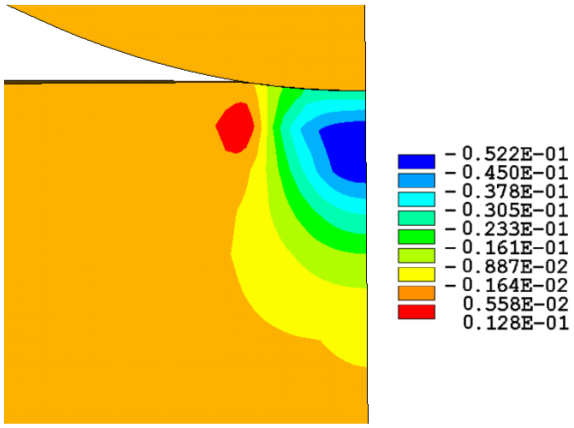

Figure 6. Plastic strain in the way of indentation [-] at the indentation depth 8.2 nm [9]. Plastic strain was calculated for the blunted Berkovich indenter, which bluntness is significant at this indentation depth.

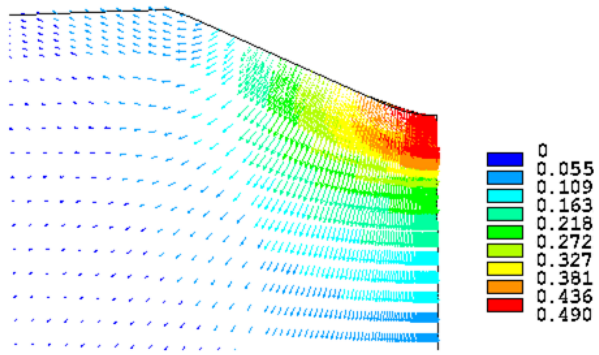

Figure 7. Total deformation [µm] at the indentation depth (displacement of indenter) 0.5 µm.

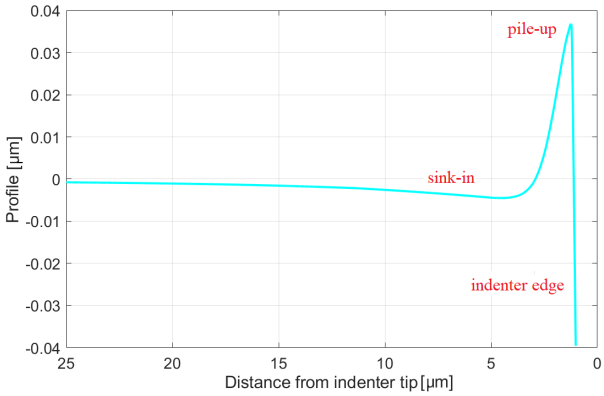

Figure 8. Detail of profile near pile-up.

Method	FEM	Oliver-Pharr	Triangular	Semi-elliptical	Parabolical
A_c [µm^2]	8.0	6.9	7.6	8.1	7.9
$\frac{\Delta A_c}{A_{cFEM}}$ [%]	–	−13.6	−4.2	1.2	−1.1

Table 1. The calculated projected contact areas and its relative difference to FEM results $\left(\frac{\Delta A_c}{A_{cFEM}}\right)$.

effect, even in the case of steel nanoindentation. The sink-in influenced calculated contact depth and this is the main reason, why its calculated value is lower than expected value.

4. Comparison of the corrections

The calculated indentation curves were analyzed using the Oliver-Pharr method. As the indenter was blunted, the projected contact area for Oliver-Pharr analysis was determined as the area of indenter cross section at the calculated contact depth ($h_c = 472\,\text{nm}$). To use corrections described in the Chapter 2.2, the height of pile-up (h_p) was measured from the end of contact depth to the maximal height of pile-up and then $h_p = 64.7\,\text{nm}$. Note that the height of pile–up is bigger that the location of its maximal point due to the sink-in described in the Chapter 3. With these values, the relations for corrections could be used and calculated values were compared in Table 1.

The boundaries of contact areas obtained for one sixth of the Berkovich indent by each approximation were plotted (Figure 9). The contact area from FEM was determined as the projected area of deformed elements, with only elements having more than half of their nodes in contact. As the mesh was fine at contact area, these results were expected to be accurate enough. The results calculated by Oliver-Pharr analysis underestimated the projected contact area approximately about 13.6 % due to the omission of the pile-up.

When the triangular correction was used, the discrepancy dropped to the 4.21 %. The triangular correction can be used to correct pile-up but it describes it inaccurately. The semi-elliptical correction overestimated the contact area about 1.16 % due to the areas near of the edge of the indenter. The parabolic correction underestimated the projected contact area about 1.07 %. Both the semi-elliptical and parabolic corrections yielded similar results and are effective for describing the pile-up region.

The knowledge of the accurate value of projected contact area is important for the determination of the Young's modulus and hardness. As the hardness is inversely proportional to the contact area and Young's modulus to its square root, the use of good correction of the projected contact area is more important for the hardness. In the same way, the influence of the corrections to Young's modulus and hardness can be determined.

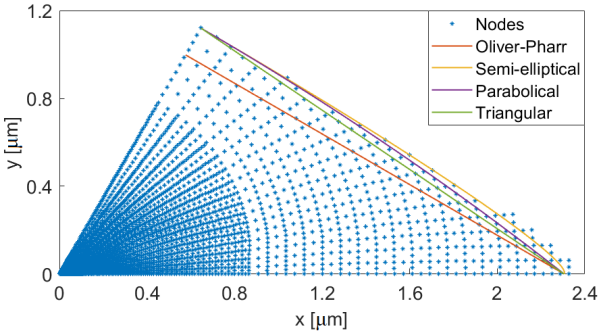

Figure 9. Comparison of the approximations of the indent boundaries with the results of FEM.

5. Conclusions

The FEM simulation of X5CrNiCoNb16-4 steel showed that the pile-up is caused by huge plastic deformation under the indenter. The plastically deformed material pushes the surrounding material upwards, creating the pile-up under the side of the indenter. Far from pile-up, the sink-in occurs, which influences the contact depth calculated by the Oliver-Pharr analysis.

The projected contact area calculated from the results of FEM calculation was compared with those calculated by Oliver-Pharr analysis and with the triangular, semi-elliptical and parabolical correction. The results showed that the Oliver-Pharr analysis underestimates projected contact area when the pile-up occurs. The triangular correction provided a better approximation of it. The most precise results were obtained by the parabolical and semi-elliptical corrections. All formulas for these corrections lead to the same dependencies, which are different by the value of the coefficient.

To get more accurate results at experimental nanoindentation, the highest point of the pile-up needs to be determined. Determination of this point is difficult due to the small scales of geometry and dimension and could be assessed in future work.

Acknowledgements

This study was realized with the support by the grant FSI-S-23-8186 and with the institutional support RVO: 61388998. JT acknowledges the support by the project OP JAC CZ.02.01.01/00/22_008/0004596 of the Ministry of Education, Youth, and Sports of the Czech Republic and EU. The language was improved by AI software ChatGPT.

References

[1] W. C. Oliver, G. M. Pharr. Measurement of hardness and elastic modulus by instrumented indentation:

Advances in understanding and refinements to methodology. *Journal of Materials Research* **19**(01):3–20, 2004. https://doi.org/10.1557/jmr.2004.19.1.3

[2] W. C. Oliver, G. M. Pharr. An improved technique for determining hardness and elastic modulus using load and displacement sensing indentation experiments. *Journal of Materials Research* **7**(06):1564–1583, 1992. https://doi.org/10.1557/JMR.1992.1564

[3] J. Kovář, V. Fuis, R. Čtvrtlík, J. Tomáštík. The influence of tilt on Berkovich indentation of a steel sample using FEM analysis and nanoindentation. *Powder Metallurgy Progress* **22**(1):53–61, 2022. https://doi.org/10.2478/pmp-2022-0007

[4] L. Fiala, I. Ballo, J. Kovář, V. Fuis. Comparison of finite element simulation of tungsten nanoindentation with Berkovich and conical indenter. In *Engineering Mechanics*, vol. 29, pp. 63–66. 2023. https://doi.org/10.21495/em2023-63

[5] J. Kovář, V. Fuis, R. Čtvrtlík. Influencing of the pile-up and the sink-in by the coefficient of friction in the nanoindentation test. In *Engineering Mechanics*, vol. 26, pp. 298–301. 2020. https://doi.org/10.21495/5896-3-298

[6] I. N. Sneddon. The relation between load and penetration in the axisymmetric Boussinesq problem for a punch of arbitrary profile. *International Journal of Engineering Science* **3**(1):47–57, 1965. https://doi.org/10.1016/0020-7225(65)90019-4

[7] J. Hu, Y. Zhang, W. Sun, T. Zhang. Nanoindentation-induced pile-up in the residual impression of crystalline Cu with different grain size. *Crystals* **8**(1):9, 2018. https://doi.org/10.3390/cryst8010009

[8] K. O. Kese, Z. C. Li, B. Bergman. Influence of residual stress on elastic modulus and hardness of soda-lime glass measured by nanoindentation. *Journal of Materials Research* **19**(10):3109–3119, 2004. https://doi.org/10.1557/JMR.2004.0404

[9] J. Kovář. *Computational modelling of nanoindentation*. Ph.D. thesis, Brno University of Technology, 2023.